CADAVERIC STUDY OF THE GREY HERON´S (ARDEA CINEREA) NASAL CAVITY AND ASSOCIATED STRUCTURES THROUGH COMPUTED TOMOGRAPHY AND ANATOMICAL SECTIONS

Student:

Natalia Roldán Medina.

Tutor:

José Raduán Jáber Mohamad.

Academic course:

2024-2025 - Ordinary call

UNIVERSIDAD DE LAS PALMAS DE GRAN CANARIA
Facultad de Veterinaria

Appreciation

First and foremost, I would like to express my deepest gratitude to my tutor and professor José Raduán Jáber Mohamad, for his invaluable support, guidance, and dedication throughout this project. I also extend my heartfelt thanks to the entire team that has worked alongside us, for their tremendous effort and commitment to this research and the others we have done before.

Furthermore, I wish to thank my family for being a constant source of strength and energy, standing by me through every moment, whether the tide was against or in favour. My deepest appreciation also goes to my boyfriend and friends, for his unconditional love and support. Without them, none of this would have been possible.

INDEX

Summary

This project aims to provide valuable insights into the anatomy of aquatic birds, focusing particularly on the respiratory system through a detailed description of the grey heron's (*Ardea cinerea*) beak and nasal system. Using anatomical cross-sections and computed tomography (CT) imaging, a comprehensive image catalogue has been created to understand the complex structures involved within the nasal cavity. This work is intended to assist biologists, veterinarians, and researchers by enhancing their knowledge of avian biology and nasal cavity physiology.

The grey heron (*Ardea cinerea)*, belonging to the Ardeidae family, is characterized by its large size, graceful flight, and specialized diet, which includes fish and small aquatic invertebrates. Structures like the nasal cavity are highly valuable as a key process for diagnosing and treating various conditions that impact the respiratory system. In this context, imaging techniques, such as computed tomography (CT), along with studies on biology and anatomy, are essential for understanding and preserving aquatic biodiversity.

Additionally, monitoring potential diseases is all-important, as these can affect domestic birds and pose a risk to public health. This approach is particularly relevant as attention to these birds increases in their natural habitat, rehabilitation centers, and zoos.

Keywords: anatomy; seabirds; grey heron; computed tomography; anatomical cross-sections; head; nasal cavity.

1. Introduction

Avian anatomy presents a suite of specialized adaptations that distinguish birds markedly from mammals, particularly in skeletal and muscular structures. These differences are the result of evolutionary pressures favoring flight, thermoregulation, and refined sensory capabilities. Among the most significant osteological divergences are elements such as the jugal and quadrate bones, which contribute to the craniofacial kinesis that permits a wide range of beak mobility (Zusi, 1993). Unlike in mammals, the angular bone persists as a distinct entity in the lower jaw of birds, playing a critical role in mandibular articulation (Starck, 1995). The epibranchial element, a vestige of ancestral branchial arches, is retained in some avian groups and contributes to the structure of the hyoid apparatus, facilitating complex tongue movements (Baumel & Witmer, 1993).

Moreover, avian skeletal structures like the coracoid and furcula (wishbone) form integral parts of the flight apparatus, serving as brace-like supports that mitigate torsional forces during wingbeats (Dial, 1992). The pygostyle, a fusion of terminal caudal vertebrae, provides anchorage for tail feathers essential in flight maneuverability and communication (Gatesy & Dial, 1996). The vomer, although reduced in birds, continues to participate in the separation of nasal and oral cavities, contributing to the complex architecture of the avian skull (König *et al*., 2014). The presence of a sclerotic ring, or scleral ossicle, encircling the eye, underscores the visual specialization of birds, providing structural support to the globe and enhancing visual acuity (Franz-Odendaal, 2006).

Another salient osteological feature of birds is the extensive pneumatization of the skeleton—an adaptation wherein air sacs invade bones, rendering them hollow and significantly lighter without compromising mechanical strength. This trait is particularly pronounced in major flight-related bones such as the humerus, sternum, and vertebrae, and is absent or rudimentary in mammals (Duncker, 1971). Pneumatization not only reduces body mass, facilitating flight, but also integrates with the avian respiratory

system, enhancing oxygen efficiency and thermoregulation during sustained aerobic activity.

In addition to these skeletal innovations, birds exhibit profound modifications in their muscular system that are fundamentally different from those of mammals. Most notably, the pectoral musculature is highly specialized for powered flight. The pectoralis major, which drives the powerful downstroke of the wing, and the supracoracoideus, which facilitates the upstroke via a unique tendon-pulley system passing through the triosseal canal, represent a functional innovation unparalleled in mammals (George & Berger, 1966). In mammals, the analogous muscles are not adapted for such cyclical, high-frequency movements and lack the specialized skeletal architecture necessary to achieve lift and thrust. Furthermore, birds show a marked reduction in epaxial musculature due to the rigid and fused nature of their vertebral column, in contrast to the more flexible axial musculature in mammals that facilitates a broader range of spinal movements (Baumel & Witmer, 1993). Avian limb musculature is similarly reduced and redistributed, allowing for lighter distal limbs and centralized body mass—a feature critical for aerial locomotion.

A particularly salient aspect of avian diversity lies in the morphology of the beak, a structure whose shape and size are finely tuned to ecological niche and dietary preference. Beaks adapted for granivory tend to be short and conical, while nectarivorous species exhibit elongated, decurved bills facilitating access to floral nectar. Carnivorous raptors possess hooked beaks for tearing flesh, whereas filter-feeding birds such as flamingos display specialized lamellae for sieving small organisms from water (Beletsky, 2007). Thus, the beak serves not only as a feeding implement but also as a functional interface with the environment, encompassing roles in grooming, manipulation, and vocalization.

Closely associated with the beak is the nasal cavity, an often-overlooked yet critical anatomical domain. In birds, the nasal cavity varies considerably in structure, ranging from simple tubular passages to complex labyrinths, depending on ecological requirements and olfactory reliance. It houses the olfactory epithelium and connects to

the respiratory system, contributing to thermoregulation, olfaction, and vocal resonance (Bang & Wenzel, 1985). The relative size and configuration of the nasal cavity can thus offer profound insights into the behavioral ecology of different avian taxa.

Given these considerations, the present study seeks to elucidate the anatomical and functional diversity of the avian nasal cavity across taxa exhibiting varied feeding ecologies. By correlating beak morphology with nasal architecture, this research aims to uncover evolutionary patterns linking cranial anatomy to ecological specialization in birds

1.1 The grey heron

The grey heron (*Ardea cinerea)*, distinguishes itself as an iconic species in the world of aquatic birds. It can reach great sizes, up to 90 centimeters in height and a wingspan of 1,70 meters (Morales-Espino *et al.*, 2024; SEO BirdLife, 2025). It can be found throughout Europe, Asia, and Africa, frequenting several environments, such as woodland, urban and suburban, marine and intertidal, farmland, wetland, and grassland (Cardarelli *et al*., 2017; Morales-Espino *et al*., 2024; Morr, 2025; SEO BirdLife, 2025). The distribution of the grey heron in Spain extends across the entire territory. Thanks to the census conducted by the Ministry of the Environment, we know that it is possible to place up to 5000 individuals during winter in just one autonomous community (Quesada-Canales *et al*., 2013).

During the breeding season, it presents a black stripe in its head, continued by two unmistakable long feathers of this same colour (Morales-Espino *et al.*, 2024; SEO BirdLife, 2025). There are no remarkable differences between the female and male individuals other than the male being somewhat larger (Garrido *et al*., 2011; Morr, 2025). They present a long beak, with a colour that varies from yellow to reddish (Boisteau & Marion, 2007; Morales-Espino *et al.*, 2024; SEO BirdLife, 2025) and a long, broad, pointed shape, which they find useful when hunting other small animals like fish, amphibians, birds or crustaceans that live in and around water (Robinson, 2005; Boisteau & Marion, 2007; Bavdek *et al*., 2017; Morale-Espino *et al.*, 2024; IUCN-SCC, 2025). The nasal cavity is located in the beak and has multiple

functions, including thermoregulation and humidification of the air, depending on the environmental conditions; filtration of particles inhaled and olfactory activity to recognise their nest and its occupants (Geist, 2000; Castelyn *et al*., 2018; Mahmoud *et al*., 2018).

Ardea cinerea is categorized as Least Concern (LC) by the IUCN Red List of Threatened Species, although in places like Thailand, Malaysia, Mauritania or Sumatra, populations have shown to be decreasing or already small enough to be concerning (Garrido *et al*., 2011; Veladiano *et al*., 2016). This species faces several risks, such as the loss of habitat, the persecution from fishermen and rice farmers, droughts, hunting and water pollution (SEO BirdLife, 2025). Thus, it is important for veterinarians, biologists and conservationists to understand the anatomy, physiology and behavior of these animals.

Furthermore, the grey heron, like many wild birds, can perform as vectors or reservoirs for viruses such as the avian influenza virus, generally asymptomatic (Faillace *et al*., 2020) or bacteria like *Mycobacterium avium,* sometimes related to signs like nasal discharge or firm white-yellowish nodules of various sizes, resembling granulomas in paranasal sinuses (Guo *et al.*, 2021; Animal´s Health, 2023). Hence it is essential to distinguish the normal anatomy of this animal's nasal cavity in order to diagnose and treat possible affectations (Yokosuka *et al*., 2009).

Since its inception, radiology has been the primary technique for investigating the nasal cavity in animals (Gibbs *et al*., 1979; Schwarz *et al*., 2000; Wilson *et al*., 2014; Kvarnemo *et al*., 2025). However, its utility is often restricted by overlapping structures, which hinder clear visualization. On the other hand, modern imaging techniques such as computed tomography (CT) have become a more precise and reliable alternative for examining animals' anatomy and associated conditions (Arencibia *et al*., 2001; De Rycke *et al*., 2003; Getty, 2004; Orosz & Lichtenberger, 2011 Bavdek *et al*., 2017; Jones *et al.*, 2019). The CT technique offers greater sensitivity and accuracy compared to traditional radiology, allowing for a more in-depth analysis of the nasal cavity. So far, the application of computed tomography (CT) to study the nasal cavity anatomy in birds

has been minimally explored in veterinary literature. While some studies have used CT to examine avian nasal anatomy, research in this area is still scarce (Burk, 1992; Veladiano *et al*., 2016; Bavdek *et al*., 2017; Aref *et al*., 2024; Kazemi *et al*., 2025; König *et al*., 2014). Thus, this research intends to describe the nasal cavity of the grey heron using both anatomical sections and CT scans.

2. Materials and Methods

2.1. Animals

To carry out this study, 3 grey herons (*Ardea cinerea*) carcasses were employed. The animals were already deceased when measured at an average weight of 1 kg (with a range of 0,8 to 1,3 kg) and an average size of 90 cm (from 85 to 92 cm) from beak to tail base. Additionally, in the skull we made measurements from the vertex of the beak to the occipital, with a length of 16 cm.

2.2. CT Technique

For CT scan evaluation, our avian subjects were thawed at ambient temperature for 12 h. Sequential transverse CT images were acquired using a 16-slice helical CT scanner (Aquilion™ Lightning, Canon Medical System®, Tokyo, Japan). The birds were placed symmetrically in dorsal recumbency on the scanner table with a craniocaudal orientation. A standard protocol was followed, applying the following parameters: 100 kVp, 90 mA, a 512 × 512 acquisition matrix, 2550 × 550 fields of view, a pitch of 0.94, and a gantry rotation time of 1.5. The obtained images had a slice thickness of 0.6 mm. To enhance the visualization of various anatomical structures in the CT images, different CT window settings were used by adjusting the window widths (WWs) and window levels (WLs): a bone window setting (WW = 1500; WL = 300), a soft tissue window setting (WW = 248; WL = 123), and a lung window setting (WW = 1400; WL = −500). No significant differences in CT density or anatomical structures were observed in the heads of the avian specimens included in this study.

2.3. Macroscopic Anatomical Sections

For a better visualization of the structures identified in the computed tomography (CT) scans, we made anatomical cross-sections. Following the CT study, the bird specimens were placed in a freezer at −80 ºC until completely frozen. Afterwards, we used an electric band saw so three carcasses were cross sectioned to obtain anatomical sequential transverse slices. Then, 1 cm cross-sections were made, starting from the beak and extending to the ocular orbit. These sections were thoroughly washed with water to eliminate any artifacts, like feathers, which were gently removed using Adson forceps. Afterward, the sections were photographed from both sides to help with the precise identification of anatomical cross-sections corresponding to the CT images.

Figure 1. Student performing the transverse cross sections.

2.4. Anatomic Evaluation

To complement and verify our identifications, we used specific anatomical literature, including textbooks, skull preparations and notable references previously described in birds, both aquatic and non-aquatic species (Codner *et al*., 1993; Boisteau & Marion, 2007; Lauridsen *et al*., 2011; Orosz & Lichtenberger, 2011; König *et al*., 2014; Bavdek *et al*., 2017; Castelyn *et al*., 2018; Madkour, 2019; Kvarnemo *et al*., 2025). The anatomical cross-sections assist us in visualizing the structures observed in the CT scans. These additional resources greatly enhanced our comprehension and ability to interpret the anatomy of the grey heron`s nasal cavity**.**

3. Results

Here we provide a lateral image of a grey heron´s head, where each numbered line corresponds to the approximate levels of the anatomical and CT cross-sections shown in the following figures. These figures include three types of images: (A) an anatomical cross-section, (B) a CT scan using the bone window setting, and (C) a CT scan using the lung window setting. The sequence of images progresses in a rostrocaudal direction, starting at the beak and continuing to the orbital fossa.

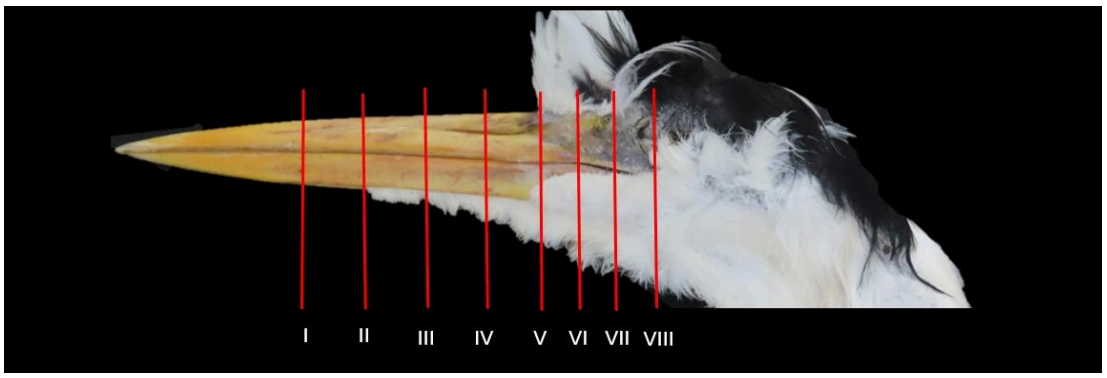

Figure 2. Anatomical (labelled with red lines) CT image corresponding to the approximate levels of the transverse slices of the grey heron´s (*Ardea cinerea*) nasal cavity.

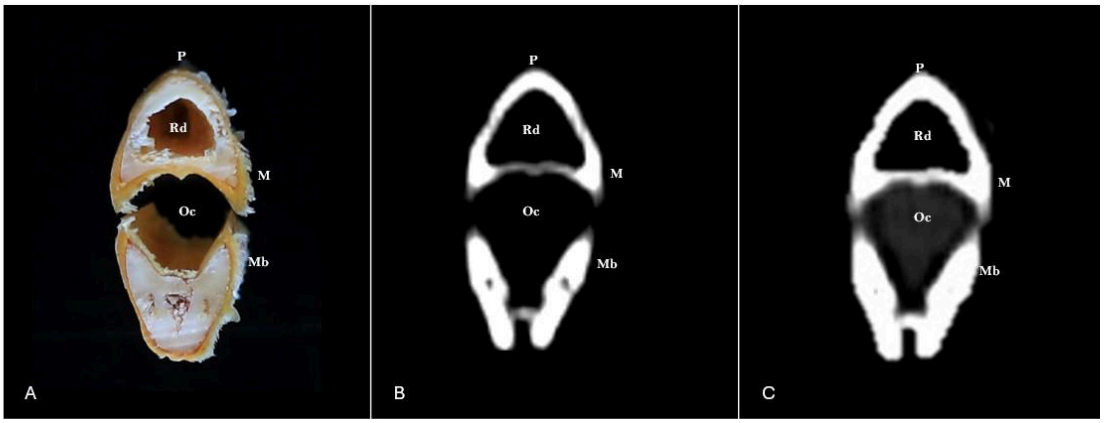

Figure 3. Transverse cross-section (A), bone window (B), and pulmonary window (C) CT images of the grey heron's nasal cavity at the level of the beak, corresponding to line I in *Figure 2*. M: maxillary bone; Mb: mandible; Oc: oral cavity; P: premaxillary bone; Rd: rostral diverticulum of the infraorbital sinus

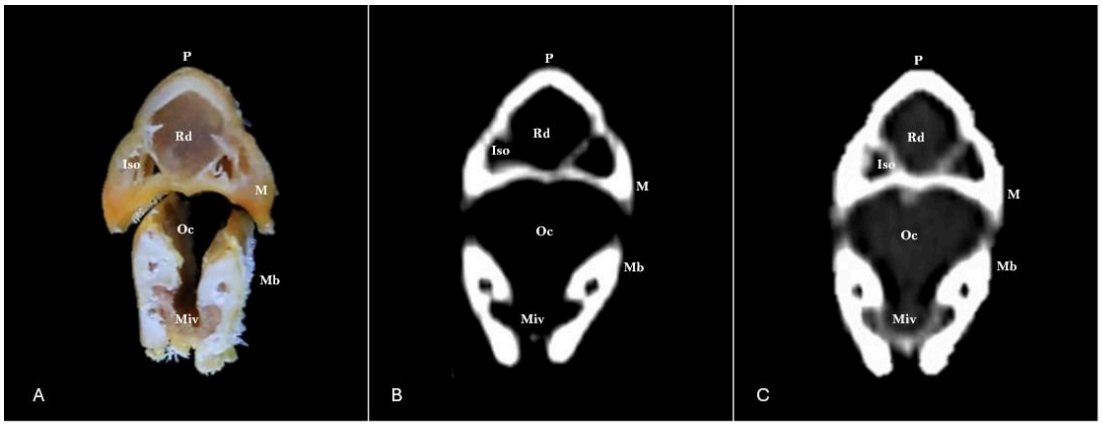

Figure 4. Transverse cross-section (A), bone window (B), and pulmonary window (C) CT images of the grey heron's nasal cavity at the level of the beak, corresponding to line II in *Figure 2*. Iso: infraorbital sinus´opening; M: maxillary bone; Mb: mandible; Miv: ventral intermandibular muscle; Oc: oral cavity; P: premaxillary bone; Rd: rostral diverticulum of the infraorbital sinus

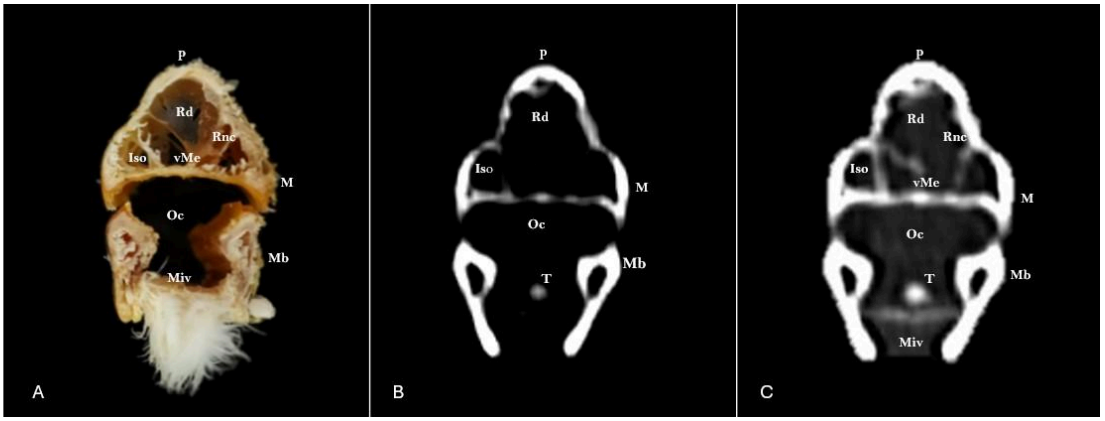

Figure 5. Transverse cross-section (A), bone window (B), and pulmonary window (C) CT images of the grey heron's nasal cavity at the level of the beak, corresponding to line III in *Figure 2*. Iso: infraorbital sinus´opening; M: maxillary bone; Mb: mandible; Miv: ventral intermandibular muscle; Oc: oral cavity; P: premaxillary bone; Rd: rostral diverticulum of the infraorbital sinus; Rnc: rostral nasal concha; T: tongue; vMe: ventral nasal meatus

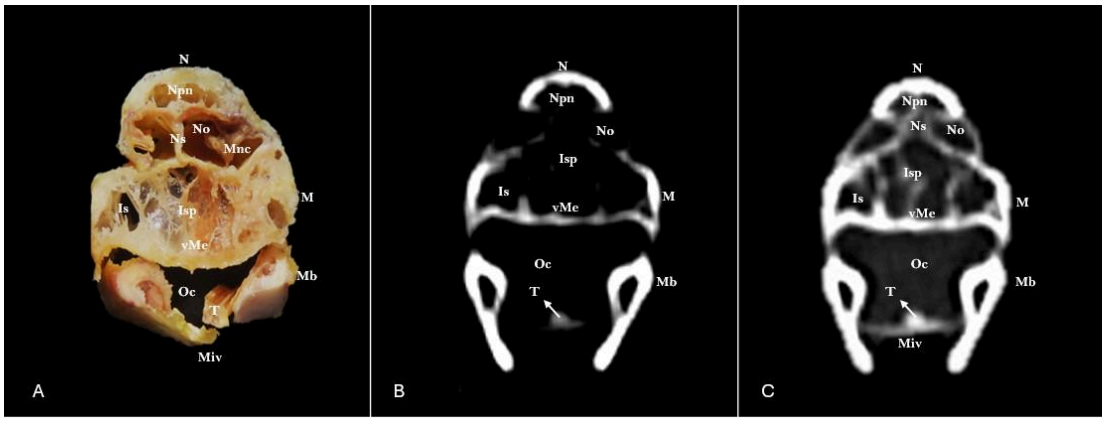

Figure 6. Transverse cross-section (A), bone window (B), and pulmonary window (C) CT images of the grey heron's nasal cavity at the level of the beak, corresponding to line IV in *Figure 2*. Is: infraorbital sinus; Isp: infraorbital sinus pneumatization; M: maxillary bone; Mb: mandible; Miv: ventral intermandibular muscle; Mnc: middle nasal concha; N: nasal bone; No: nostrils; Npn: nasal bone pneumatization; Ns: nasal septum; Oc: oral cavity; T: tongue; vMe: ventral nasal meatus

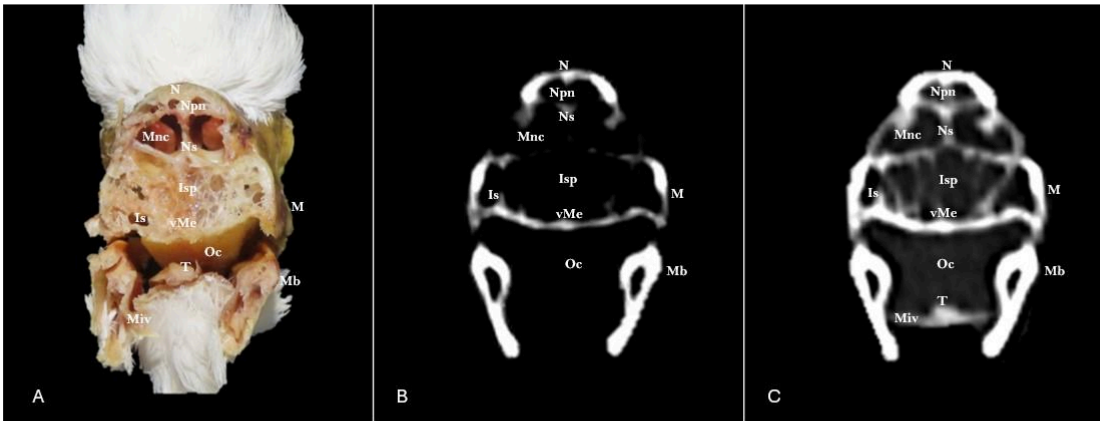

Figure 7. Transverse cross-section (A), bone window (B), and pulmonary window (C) CT images of the grey heron's nasal cavity at the level of the beak, corresponding to line V in *Figure 2*. Is: infraorbital sinus; Isp: infraorbital sinus pneumatization; M: maxillary bone; Mb: mandible; Miv: ventral intermandibular muscle; Mnc: middle nasal concha; N: nasal bone; Ns: nasal septum; Oc: oral cavity; T: tongue; vMe: ventral nasal meatus

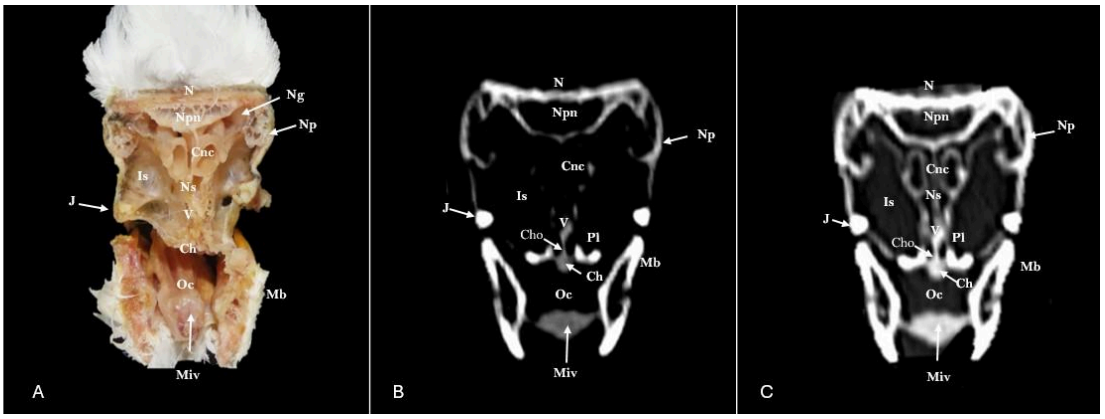

Figure 8. Transverse cross-section (A), bone window (B), and pulmonary window (C) CT images of the grey heron's nasal cavity at the level of the beak, corresponding to line VI in *Figure 2.* Ch: choanal cleft; Cho: choanal opening; Cnc: caudal nasal concha; Is: infraorbital sinus; J: jugal bone; Mb: mandible; Miv: ventral intermandibular muscle; N: nasal bone; Ng: nasal gland; Np: nasal process; Npn: nasal bone pneumatization; Ns: nasal septum; Oc: oral cavity; Pl: palatine bone; V: vomer

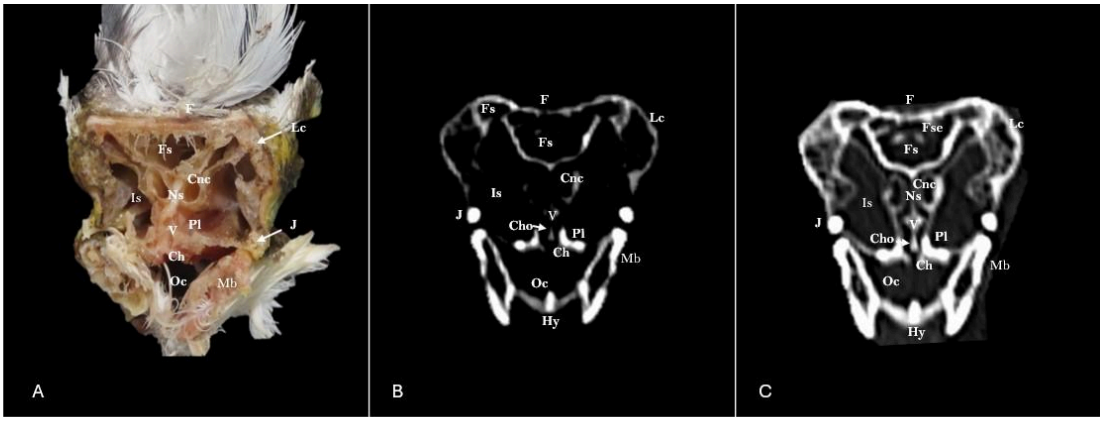

Figure 9. Transverse cross-section (A), bone window (B), and pulmonary window (C) CT images of the grey heron's nasal cavity at the level of the beak, corresponding to line VII in *Figure 2*. Ch: choanal cleft; Cho: choanal opening; Cnc: caudal nasal concha; F: frontal bone; Fs: frontal sinus; Fse: frontal septum; Hy: hyoid apparatus; J: jugal bone; Lc; lacrimal bone; Mb: Mandible; Ng: Nasal gland; Ns: Nasal septum; Oc: Oral cavity; Pl: palatine bone; V: vomer

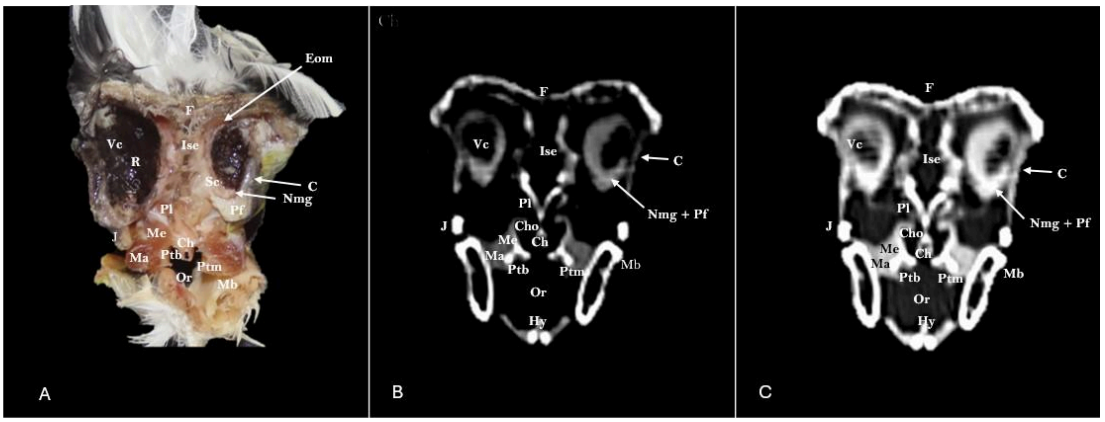

Figure 10. Transverse cross-section (A), bone window (B), and pulmonary window (C) CT images of the grey heron's nasal cavity at the level of the beak, corresponding to line VIII in *Figure 2*. C: cornea; Ch: choanal cleft; Cho: choanal opening; Em: extraocular muscle (superior oblique muscle); F: frontal bone; Hy: hyoid apparatus; Ise: interorbital septum; J: jugal bone; L: lens; Ma: mandibular adductor externus ventralis muscle; Mb: Mandible; Me: ethmomandibular muscle; Nmg: nictitating membrane gland; Or: Oropharynx; Pf: periorbital fat; Pl: palatine bone; Ptb: pterygoid bone; Ptm: pterygoid muscle; R: retina; Sc: sclera; Vc: vitreous chamber

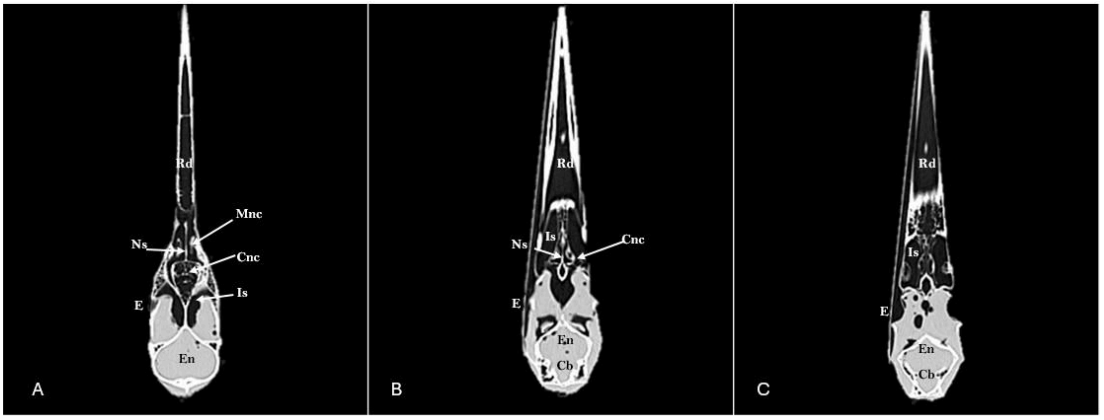

Figure 11. Dorsal view of a pulmonary and soft-tissue algorithm CT images of the grey heron's head at different levels. Cb: cerebelar body; Cnc: caudal nasal concha; E: eyeball; En: encephalon; Is: infraorbital sinus; Mnc: medial nasal concha; Ns: nasal septum; Rd: rostral diverticulum of the infraorbital sinus

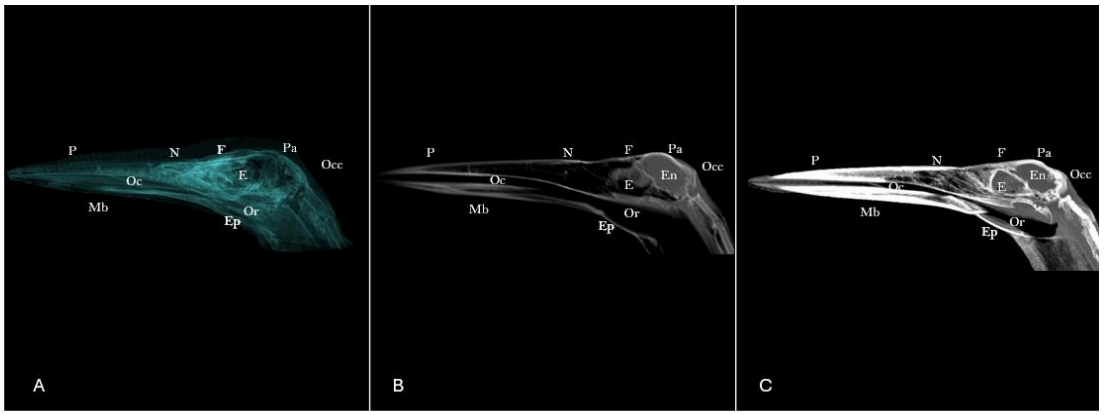

Figure 12. Sagittal view using OsiriX MIP reconstructed CT image (A) bone window (B), and pulmonary window (C) CT images of the grey heron's head. E: eyeball; En: encephalon; Ep: epibranchial bone; F: frontal bone; Mb: mandible; N: nasal bone; Oc: oral cavity; Occ: occipital bone; Or: oropharynx; P: premaxillary bone; Pa: parietal bone

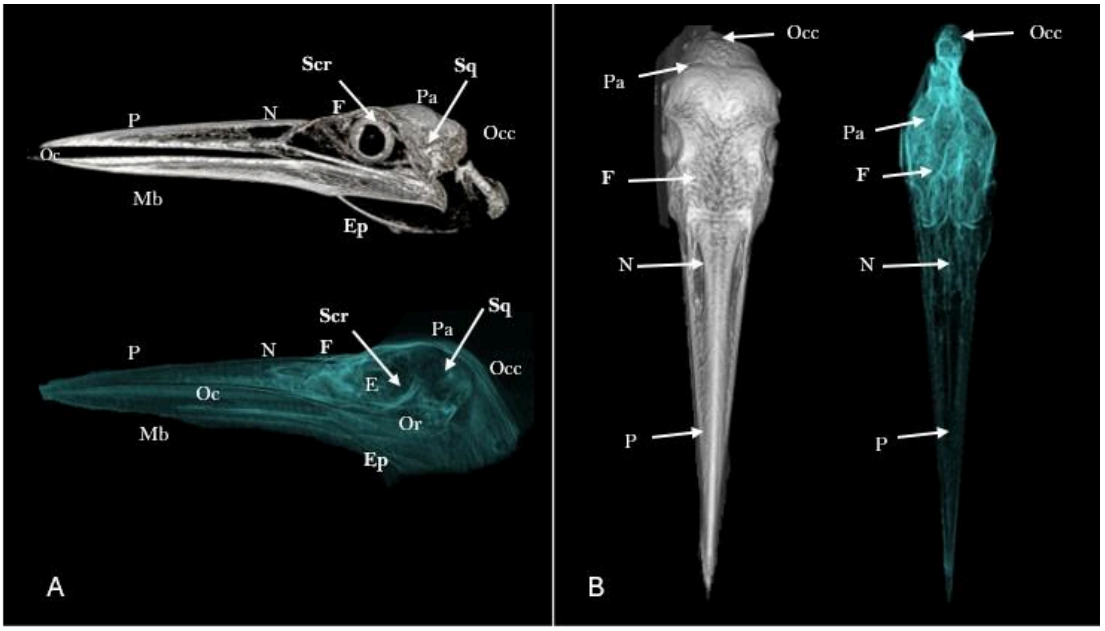

Figure 13. Lateral view (A) and dorsal view (B) using OsiriX MIP reconstructed and volume rendering (VR) CT images of the grey heron's head. E: eyeball; Ep: epibranchial bone; F: frontal bone; Mb: mandible; N: nasal bone; Oc: oral cavity; Occ: occipital bone; Or: oropharynx; P: premaxillary bone; Pa: parietal bone; Scr: scleral ring; Sq: squamosal bone

3.1. Anatomical Sections

We identified clinically relevant structures of the nasal cavity using anatomical cross-sections. Therefore, the selected slices displayed key anatomical landmarks of this cavity, which extends from the nostrils to the choanal slit. As in other birds, the nostrils (subfigure A in *Figure 6* and *Figure 7*) were located at the base of the beak. Transversal images allowed for the visualization of the nasal septum (subfigure A in *Figures 6*, *Figure 7*, *Figure 8 and Figure 9)*, which separates the left and right nasal cavities.

The floor of the nasal cavity was supported rostrally by the palatine processes of the maxilla, while caudally it was comprised of the thin palatine bone (subfigure A in *Figure 9* and *Figure 10*) and vomer (subfigure A in *Figure 8* and *Figure 9*). The nasal cavity roof was formed rostrally by the premaxillary (subfigure A in *Figure 3*, *Figure 4* and *Figure 5*), nasal (subfigure A in *Figure 6*, *Figure 7* and *Figure 8*) and maxillary bones (subfigure A in *Figure 3*, *Figure 4*, *Figure 5*, *Figure 6* and *Figure 7)*, and more caudally by the frontal (subfigure A in *Figure 9* and *Figure 10*) and lacrimal bone (subfigure A in *Figure 9*). The nasal bone also exhibited a nasal process (subfigure A in *Figure 8)* and visible nasal pneumatization in some slices (subfigure A in *Figure 6*, *Figure 7 and Figure 8)*. Other bones were distinguishable throughout the cross-sections, including the mandible (subfigure A in *Figure 3*, *Figure 4*, *Figure 5*, *Figure 6*, *Figure 7*, *Figure 8*, *Figure 9* and *Figure 10*) jugal (subfigure A in *Figure 8*, *Figure 9 and Figure 10)* and the pterygoid bone (subfigure A in *Figure 10*).

Cross-sections showed the cone-shaped nasal cavity, whose apex pointed rostrally and was caudally composed of three nasal conchae: rostral (subfigure A in *Figure 5*), middle (subfigure A in *Figure 6* and *Figure 7*), and caudal (subfigure A in *Figure 8* and *Figure 9*). The rostral nasal concha had a smooth, flat medial surface. The middle nasal concha, the largest in size, appeared caudal to the rostral one. The caudal nasal concha, located rostrally to the eye, connected to the infraorbital sinus (subfigure A in *Figure 6*, *Figure 7*, *Figure 8* and *Figure 9*) rather than the nasal cavity. This sinus occupied a triangular space within the maxillary bone, where the opening (subfigure A in *Figure 4* and *Figure 5*) and the rostral diverticulum of the sinus can be distinguished (subfigure A in *Figure 3*, *Figure 4* and *Figure 5*), and extended rostroventrally to the eye, exhibiting

pneumatization with a trabeculated pattern across multiple segments of its extent (subfigure A in *Figure 6* and *Figure 7*). The interorbital sinus (subfigure A in *Figure 10*) was also visible in the medial region between the orbits. Between the nasal conchae and the nasal cavity walls were the nasal meatuses (subfigure A in *Figure 5*, *Figure 6* and *Figure 7*). The nasolacrimal duct was supposed to be between the middle nasal conchae and curved over the dorsal aspect of the infraorbital sinus, but clear observation was hindered by the minute size of the structures.

These anatomical views also highlighted formations of the oral cavity (subfigure A in *Figure 3*, *Figure 4*, *Figure 5*, *Figure 6*, *Figure 7*, *Figure 8* and *Figure 9*), including the tongue (subfigure A in *Figure 6* and *Figure 7*) and oropharynx (subfigure A in *Figure* 10). The choanal cleft (subfigure A in *Figure 8*, *Figure 9* and *Figure 10*) , connecting the nasal cavity to the oral cavity, displayed a slit-like shape rostrally and a triangular configuration caudally. It lay between the palatine bones and was dorsally bordered by the vomer and nasal septum. Soft tissue structures were easily discernible, such as the nasal gland (subfigure A in *Figure 8*), located medially to the lacrimal bone and rostrally adjacent to the nasal and frontal bones. This gland releases secretions into the nasal vestibule. Other elements included the hyoid apparatus, that was only visualized on the CT images, and the gland of the nictitating membrane (subfigure A in *Figure 10*).

Muscular structures were also well defined, including the ventral intermandibular muscle (subfigure A in *Figure 4*, *Figure 5*, *Figure 6*, *Figure 7*, and *Figure 8*), pterygoid muscle (subfigure A in *Figure 10*), ethmomandibular muscle (subfigure A in *Figure 10*), and the mandibular adductor externus ventralis muscle (subfigure A in *Figure 10*). The extraocular muscles surrounding the eyeball were clearly visible, along with the surrounding periorbital fat (subfigure A in *Figure 10*). Additionally, cross-sections facilitated the observation of various orbital components, such as the vitreous chamber, the retina, the sclera, or the cornea.

3.2. Computed Tomography (CT)

No relevant differences were detected with the CT technique between the three grey herons. CT images were useful to identify some important structures and differentiate them, with a clear hyperattenuation on bones and hypoattenuation on other structures in both pulmonary and bone CT windows. For instance, the rostral diverticulum of the infraorbital sinus is a hypoattenuated structure that steers through the premaxillary bone until the nasal septum (subfigures B, C in *Figure 3*, *Figure 4* and *Figure 5* and subfigures A, B, C in *Figure 11*). Another structure with this attenuation is shown along the nasal cavity is the infraorbital sinus, which grows in size caudally (subfigures B, C in *Figure 4*, *Figure 5*, *Figure 6*, *Figure 7*, *Figure 8* and *Figure 9* and subfigures A, B, C in *Figure 11*). Similar attenuation characteristics were observed in the nostrils (subfigures B, C in *Figure 6*)

Furthermore, with a slightly more hyperattenuation, the tongue could be appreciated in the oral cavity (subfigures B, C in *Figure 5*, *Figure 6*, and subfigure C in *Figure 7*). Ventrally, we can see the ventral intermandibular muscle (subfigures B, C in *Figure 4*, *Figure 8* and subfigure C in *Figure 5*, *Figure 6* and *Figure 7*). Between all these structures we appreciated with a hypoattenuation the ventral nasal meatus (subfigures B, C in *Figure 6* and *Figure 7* and subfigure C in *Figure 5*). Additionally, we could see the rostral nasal concha (subfigure C in *Figure 5*), the medium nasal concha (subfigures B, C in *Figure 7* and subfigure A in *Figure 11*) and the caudal nasal concha (subfigures B, C in *Figure 8* and *Figure 9* and subfigure B in *Figure 11*) although the pulmonary CT window was more distinctive. Likewise, the choanal cleft and opening were clearly visible (subfigures B, C in *Figure 8*, *Figure 9* and *Figure 10*).

In addition, muscles such as the mandibular adductor externus ventralis and the pterygoid muscle were identified (subfigures B, C in *Figure 10*). In addition, structures of the eye were recognizable as the vitreous chamber, the cornea, the nictitating membrane gland and the periorbital fat (subfigures B, C in *Figure 10*). Finally, the CT technique was useful in the identification of different skull bones, such as the premaxillary (subfigures B, C, in *Figure 3*, *Figure 4* and *Figure 5*), maxillary (subfigures B, C, in *Figure 3, Figure 4*, *Figure 5, Figure 6* and *Figure 7*), mandible

(subfigures B, C, in *Figure 3*, *Figure 4*, *Figure 5*, *Figure 6*, *Figure 7*, *Figure 8*, *Figure 9* and *Figure 10*), nasal (subfigures B, C in *Figure 6*, *Figure 7* and *Figure 8*), jugal (subfigures B, C in *Figure 8, Figure 9 and Figure 10*), palatine (subfigures B, C in *Figure 8, Figure 9 and Figure 10*), vomer (subfigures B, C in *Figure 8* and *Figure 9*), pterygoid (subfigures B, C in *Figure 10*) and frontal bones (subfigures B, C in *Figure* 9 and *Figure 10*), which appeared with hyperattenuation in both pulmonary and bone CT windows.

Three-dimensional reconstructions were also carried out using the OsiriX software, which enabled the generation of 3D images and different views (dorsal and lateral) that provided valuable insights into the identification of anatomical structures. These reconstructions, along with the various CT window settings, offered an alternative perspective, allowing for a more comprehensive assessment and deeper understanding of the identifications made throughout the study. Among the structures identified were various cranial bones, including the squamosal bone (subfigure A in *Figure 13*), the premaxillary, maxillary, nasal, frontal, parietal and occipital bones, comprised of its basioccipital, exoccipital, and supraoccipital portions, as well as the mandible and the epibranchial bone, a component of the hyobranchial apparatus (subfigures A, B, C in *Figure* 12 and subfigure A in *Figure 13*). In addition, other structures such as the encephalon (subfigures A, B, C in *Figure* 11 and subfigures B, C in *Figure 12*), cerebellum (subfigures B, C in *Figure 11*), eye (subfigures A, B, C in *Figure* 11 and *Figure 12* and subfigure A in *Figure 13*), the scleral ring (subfigure A in *Figure 13*), oral cavity, and oropharynx (subfigures A, B, C in *Figure* 12 and subfigure A in *Figure 13*) were clearly distinguishable.

4. Discussion

Herons are widely distributed wading birds that inhabit diverse aquatic and semi-aquatic ecosystems across the globe. Despite their adaptability, these birds face various natural and anthropogenic threats. Therefore, climatic events such as the El Niño phenomenon have been associated with increased flooding, often resulting in the destruc-tion of nests and reduced breeding success (Fasola *et al*., 2009). In addition, *Clostridium botulinum* proliferates easily in warm and stagnant waters, common habitats for grey herons.

Other relevant anthropogenic factors include collisions with electrical wires and secondary poisoning from rodenticides ingested by small prey within their diet (Sandoval, 2000; Ogórek *et al*., 2022; Martínez *et al*., 2024). Interestingly, a recent study has demonstrated signs of recovery among grey heron populations probably due to their ecological plasticity and wide distribution (Diario de Gran Canaria, 2025). Nonetheless, long migratory journeys undertaken during breeding and nesting seasons can lead to considerable muscular fatigue and physiological stress, further affecting their survival and reproductive performance. Given the wide range of environmental pres-sures and physiological demands grey herons are exposed to, particu-larly those related to their aquatic lifestyle and migratory behaviour, understanding their cranial anatomy becomes essential. Specific ana-tomical adaptations may play a crucial role in their ability to regulate temperature, pressure, and respiration in fluctuating and often chal-lenging habitats.

This study presents anatomically relevant findings, as the nasal cavity of this species has not been previously described. Our observations reveal distinct morphological differences compared to both aquatic and terrestrial bird species. These results contribute valuable insights into the comparative anatomy of avian respiratory systems and underscore the need for further investigation into species-specific adaptations.

To begin with, the infraorbital sinus is characterized by a complex network of interconnected cavities, a structure that differs markedly from its mammalian counterparts. The different CT windows and planes used in this study were quite helpful in identifying this sinus, and its extension from the rostral nasal concha to the ventral side of the eyeball. Although the precise function of the infraorbital sinus remains unclear, some studies conducted in Cory's Shearwater (Morales-Espino, 2024) and ostrich (Aref *et al*., 2024)suggest that certain bird species may be capable of directing airflow through parts of this sinus. Interestingly enough, investigations performed in aquatic birds pointed out that the infraorbital sinus could play a role in regulating pressure during diving and thermoregulation (Burk, 1992; Yokosuka *et al.*, 2009; Porter & Witmer, 2016 Bavdek *et al*., 2017).

Although the Grey Heron is an aquatic species commonly found in wetlands, rivers, lagoons, marshes and estuaries, in both freshwater and brackish environments, it does not forage in open marine waters. As consequence, it lacks the specialized anatomical adaptations observed in true seabirds, such as highly developed nasal glands for salt excretion, as demonstrated using anatomical sections and CT imaging (Dunson *et al*., 1971; Shuttleworth *et al*., 1987; Franklin & Grigg, 1993; Babonis & Evans, 2011; Grossel *et al*., 2020). For the aforementioned reasons, it was hard to clearly identify the gland due to the underdevelopment of it and the lack of sensitivity regarding soft tissue of the CT scan. Only the caudal portion of the gland was visualized at the transition between the nasal bone and the frontal bone. Its rostral extent and relationship with adjacent structures were not well defined in our images. These findings may vary slightly in morphology, size, and arrangement depending on the species.

Concerning the nasal septum, it serves to divide the nasal cavity into two distinct passages, showing a general structural pattern comparable to that of other avian and mammalian species (Basha *et al*., 2022). Our observations revealed a caudal extension of the septum. This feature became evident through the combined use of transverse anatomical cross-sections and CT imaging, which also allowed for clear identification of the septal sinus. Unlike in some species where this sinus appears as a single bony cavity, in the Grey Heron it appeared as a more defined and distinguishable space. An ob-servation that, while not universal across all birds, has been reported in other species according to previous studies (Burk, 1992; Aref *et al*., 2024; Kazemi *et al*., 2025).

Within the nasal cavity, the nasal conchae (or turbinates) were arranged in a rostro-caudal orientation, spanning from the anterior to the posterior regions. Due to this linear configuration, the commonly used mammalian terms for nasal meatuses (dorsal, middle, and ventral) do not accurately apply. The rostral nasal concha was reduced in size compared to other species. Consistent with findings in both aquatic and terrestrial bird species such as the chicken, turkey, ostrich, amazon parrot, pigeon, duck, goose, and puffin, the middle nasal concha was the most developed (Burk, 1992; Stańczyk *et al*., 2018; Aref *et al*., 2024; Kazemi *et al*., 2025).

The juxtaposition of CT and anatomical images validated the interpretation of nasal anatomy. Structures that appeared ambiguous in one modality were clarified using the complementary technique. For instance, the medial nasal concha, difficult to isolate in CT due to similar densities, was clearly identifiable in the anatomical sections. This comparative method enhanced accuracy in labelling anatomical features and understanding their clinical relevance.

The olfactory epithelium in birds, including species like the grey heron, is a specialized tissue located in the nasal cavity, primarily lining the caudal nasal conchae. The olfactory system in birds, though generally less developed than in mammals, varies among species and plays roles in behaviors such as foraging, navigation, and social interactions (Hadden *et al.*, 2022). CT scans have been effective in highlighting the anatomical relationship between the caudal nasal concha and the infra-orbital sinus, aiding in the understanding of the olfactory system's structure and function in this species (Arienzo *et al*., 2023).

The choana is a key anatomical feature within the nasal cavity. In birds and reptiles, it is associated with the incomplete development of the secondary palate. Birds do not have a distinct nasopharynx, instead, the nasal cavity communicates directly with the oropharynx through the choana, without a clear anatomical separation. Its closure occurs during swallowing, and it allows the connection between the nasal and oral cavities (Sandoval, 2000). In aquatic bird species, the morphology of the choana displays slight variations. Instead of the commonly reported oval shape described in terrestrial species, the choana appeared more elongated, resembling that observed in other seabirds like Cory’s Shearwater (Morales-Espino, 2024). This was clearly seen in both anatomical cross-sections and CT scans. Clinically, the choanal cleft offers a significant advantage by providing direct endoscopic access to the nasal cavity, enabling accurate internal examination (Sandoval, 2000). It also facilitates efficient sampling, which is essential for diagnosing and monitoring respiratory infections and other diseases in birds (Porter & Witmer, 2016; Hadden *et al.*, 2022).

The vomeronasal organ is a key chemosensory structure in many vertebrates, involved in detecting pheromones and predator odors. In reptiles, it triggers defensive behaviors and assists in prey tracking, while in mammals, it mediates responses to predator scents, although the specific sensory neurons involved remain unfortunately unidentified to date. Although a rudimentary form appears during embryonic development in birds, it regresses before maturity, rendering it vestigial rather than functional (Papes *et al.*, 2010). This differs from some aquatic and terrestrial vertebrates, where the organ is retained and plays important ecological roles (Castelyn *et al*., 2018) The persistence of the vomer alongside the loss of a functional sensory organ reflects birds' evolutionary history, whereas the retention of the organ in other species illustrates adaptations to diverse environmental demands.. In our study, we observed the presence of the vomer bone, which provides structural support within the nasal cavity despite the absence of a functional vomeronasal organ in birds.

In contrast to many terrestrial bird species that possess a nasal operculum, a cartilaginous or keratinized structure that can partially cover the nostrils, aquatic birds have evolved alternative anatomical adaptations suited to their aquatic environments. These modifications enhance respiratory efficiency and protect the nasal passages during prolonged submersion. Instead, these birds exhibit elongated and flattened nostrils, which facilitate diving and help prevent water ingress.

One key limitation of this study lies in the fact that all the specimens analyzed were juveniles. Age can significantly influence anatomical development, and studies in mammals have shown that nasal structures can undergo considerable growth in both length and width during maturation (Kazemi *et al*., 2025). Additionally, the presence of down feathers in some of the specimens, which aid in thermoregulation, emphasizes their early developmental stage. Since the nasal cavity also plays important roles in air humidification, filtration, water conservation, and temperature regulation (Papes *et al.*, 2010; Garrido *et al*., 2011; Quesada-Canales *et al*., 2013; Animal´s Health, 2023; IUCN-SCC, 2025). This suggests that the findings presented here may not fully represent the anatomy of adult individuals. To improve anatomical accuracy and obtain comprehensive morphometric data, it would be necessary to carry out comparative studies using both juvenile and adult birds.

In this study, we selected the CT images that best corresponded to the anatomical cross-sections. Sequential transverse images revealed the internal structure of the nasal cavity, and the anatomical integrity of the bony nasal passage was preserved in all three specimens. As reported in previous investigations (Burk, 1992), the quality of nasal cavity imaging tends to improve with the physical size of the beak, as seen in the grey heron, whose larger beak volume allowed for better image resolution when compared to other species studied (König *et al*., 2014; Bavdek *et al*., 2017; Sovrano *et al*., 2019; Fumero-Hernández *et al*., 2023; Aref *et al*., 2024; Kazemi *et al*., 2025). This relationship between specimen size and image quality is particularly relevant when considering the technical limits of the imaging equipment. However, in our case, the CT images still presented limitations in resolution, likely due to the relatively low tissue volume and the small dimensions of the nasal cavity (measuring around 15 cm from the beak to the rostral orbit, but only 1 to 3 cm in height along the rhamphotheca) which made image acquisition especially challenging, being almost impossible to identify structures such as the ophthalmic division of the trigeminal nerve, which is observed in other studies with bigger specimens or higher resolution (Wild & Zeigler, 1996; Williams & Wild, 2001; Papes *et al.*, 2010). It is important to note that in the CT evaluation, the lung window setting provided better delineation of certain anatomical structures, enhancing the overall visualization within the nasal cavity.

The use of OsiriX software was instrumental in enhancing the anatomical visualization of the nasal cavity. By enabling post-processing of DICOM images through maximum-intensity projection (MIP) and volume-rendering techniques, OsiriX provided three-dimensional reconstructions that allowed for a more accurate and realistic identification of internal and external structures. This three-dimensional visualization proved particularly valuable given the anatomical complexity and small size of the nasal cavity, which posed challenges for interpretation using conventional two-dimensional CT slices. The enhanced spatial perception offered by OsiriX not only improved anatomical understanding but also contributed significantly to the potential for future applications in diagnostic imaging and surgical planning.

These difficulties could potentially be mitigated using micro-computed tomography (micro-CT), which has demonstrated superior resolution in studies involving other exotic species. Despite its advantages, micro-CT remains largely inaccessible in routine veterinary practice due to its cost and technical demands, limiting its use to research centers or institutions with advanced imaging capabilities (Hadden *et al.*, 2022; Kazemi *et al*., 2025). The combination of CT scans and anatomical cross-sections nonetheless allowed for the observation of the structural boundaries and configuration, which is essential for diagnostic purposes and may be applicable to other avian species.

5. Conclusions

This investigation provides the first detailed anatomical description of the nasal cavity of the grey heron (*Ardea cinerea*) using computed tomography (CT) images in transverse, sagittal, and dorsal planes, in conjunction with anatomical cross-sections. The images obtained in this study proved to be highly valuable in identifying precise anatomical landmarks and spatial relationships within the nasal cavity. As a result, the information gathered can assist veterinary clinicians in recognizing and diagnosing various pathological conditions affecting this region in herons. Furthermore, the integration of advanced imaging techniques into anatomical research offers significant educational potential for veterinary students and residents by enabling the visualization of complex structures without superimposition. This facilitates a clearer understanding of the intricate organization of the rostral head in avian species. Ultimately, a comprehensive understanding of the species-specific anatomy of the nasal cavity enhances our ability to detect, evaluate, and manage diseases that may compromise this area. Such an approach is instrumental in improving diagnostic accuracy and advancing therapeutic strategies tailored to the unique anatomical features of the grey heron.

6. Bibliography

- *Ardea cinerea*: BirdLife International. (2016). In IUCN Red list of threatened species. https://doi.org/10.2305/iucn.uk.2016-3.rlts.t22696993a86464489.en

- Aref, M., Raouf, M. a. E., Youssef, W. O. M., Abdelbaset-Ismail, A., Salem, G. A., Nassan, M. A., Rutland, C. S., & Mahdy, E. a. A. (2024). Structural investigations of the normal ostrich head using anatomical sections, computed tomography, and magnetic resonance imaging Open Veterinary Journal, 14(12), 3487. https://doi.org/10.5455/ovj.2024.v14.i12.32 (Aref et al., 2024)

- Arencibia, A., Vazquez, J. M., Ramirez, J. A., Ramirez, G., Vilar, J. M., Rivero, M. A., Alayon, S., & Gil, F. (2001). MAGNETIC RESONANCE IMAGING OF THE NORMAL EQUINE BRAIN. Veterinary Radiology & Ultrasound, 42(5), 405–408. https://doi.org/10.1111/j.1740-8261.2001.tb00959.x (Arencibia et al., 2001)

- Arienzo, M., Toscanesi, M., Esposito, M., Iaccarino, D., Di Nocera, F., Canzanella, S., Ferrara, L., Di Natale, G., & Trifuoggi, M. (2023). Comparative study of polycyclic aromatic hydrocarbons (PAHs) in salt gland and liver of loggerhead turtle Caretta caretta (Linnaeus, Cheloniidae) stranded along the Mediterranean coast, Southern Italy. Ecotoxicology and Environmental Safety, 263, 115355. https://doi.org/10.1016/j.ecoenv.2023.115355 (Arienzo et al., 2023)

- Babonis, L. S., & Evans, D. H. (2011). Morphological and biochemical evidence for the evolution of salt glands in snakes. Comparative Biochemistry and Physiology Part a Molecular & Integrative Physiology, 160(3), 400–411. https://doi.org/10.1016/j.cbpa.2011.07.008 (Babonis and Evans, 2011)

- Basha, W. a. A., Farouk, S. M., & Hassan, S. a. M. (2022). Anatomical, histochemical and surface ultrastructural characteristics of cavum nasi of the common quails (Coturnix coturnix. Erlangeri). Anatomia Histologia Embryologia, 51(4), 468–476. https://doi.org/10.1111/ahe.12808 (Basha et al., 2022)

- Baumel, J. J. (1993). Handbook of Avian Anatomy: Nomina Anatomica Avium. Harvard Univ Nuttall ornithological.

- Bavdek, S. V., Golob, Z., Janžekovič, F., Rutland, C. S., & Kubale, V. (2017). Skull of the grey heron (*Ardea cinerea*): Detailed investigation of the orbital region. Anatomia Histologia Embryologia, 46(6), 552–557. https://doi.org/10.1111/ahe.12308 (Bavdek et al., 2017)

- Beletsky, L. (2007). Collins. Birds of the World. Collins Publishers.

- Bock, W. J. (1967). Avian Myology J. C. George A. J. Berger. Ornithology, 84(1), 138–140. https://doi.org/10.2307/4083275

- Boisteau, B., & Marion, L. (2007). Habitat use by the Grey Heron (*Ardea cinerea*) in eastern France. Comptes Rendus Biologies, 330(8), 629–634. https://doi.org/10.1016/j.crvi.2007.05.006 (Boisteau and Marion, 2007)

- Burk, R. L. (1992). COMPUTED TOMOGRAPHIC ANATOMY OF THE CANINE NASAL PASSAGES. Veterinary Radiology & Ultrasound, 33(3), 170–176. https://doi.org/10.1111/j.1740-8261.1992.tb01440.x (Burk, 1992)

- Cardarelli, E., Fasola, M., Martinoli, A., & Pellitteri-Rosa, D. (2017). Long-Term Changes in Food Intake by Grey Herons (*Ardea cinerea*), Black-Crowned Night-Herons (Nycticorax nycticorax) and Little Egrets (Egretta garzetta) Foraging in Rice Fields in Italy. Waterbirds, 40(4), 344–352. https://doi.org/10.1675/063.040.0406

- Casteleyn, C., Cornillie, P., Van Cruchten, S., Van Den Broeck, W., Van Ginneken, C., & Simoens, P. (2018). Anatomy of the upper respiratory tract in domestic birds, with emphasis on vocalization. Anatomia Histologia Embryologia, 47(2), 100–109. https://doi.org/10.1111/ahe.12336

- Codner, E., Lurus, A., Miller, J., Gavin, P., & Barbee, D. (1993, April 1). Comparison of computed tomography with radiography as a noninvasive diagnostic technique for chronic nasal disease in dogs. PubMed. https://pubmed.ncbi.nlm.nih.gov/8473224/

- Davies, M. N., & Green, P. R. (2012). Perception and motor control in birds: An Ecological Approach. Springer Science & Business Media.

- De Rycke, L. M., Saunders, J. H., Gielen, I. M., Van Bree, H. J., & Simoens, P. J. (2003). Magnetic resonance imaging, computed tomography, and cross-sectional views of the anatomy of normal nasal cavities and paranasal sinuses in mesaticephalic dogs. American Journal of Veterinary Research, 64(9), 1093–1098. https://doi.org/10.2460/ajvr.2003.64.1093

- Dial, K. P. (1992). Activity patterns of the wing muscles of the pigeon (Columba livia) during different modes of flight. Journal of Experimental Zoology, 262(4), 357–373. https://doi.org/10.1002/jez.1402620402

- Duncker, H. (2013). The lung air sac system of birds: A contribution to the functional anatomy of the respiratory apparatus. Springer Science & Business Media.

- Dunson, W. A., Packer, R. K., & Dunson, M. K. (1971). Sea Snakes: An Unusual Salt Gland under the Tongue. Science, 173(3995), 437–441. https://doi.org/10.1126/science.173.3995.437

- El Centro de Fauna Silvestre atiende a una garza real que llegó débil e inmóvil por botulismo. (2020, October 22). Diario De Gran Canaria. https://diariodegrancanaria.opennemas.com/articulo/gran-canaria/centro-fauna-silvestre-garza-real/20201021202431002067.html

- Faillace, A. C. L., Vieira, K. R. A., & Santana, M. I. S. (2020). Computed tomographic and gross anatomy of the head of the blue‐fronted Amazon parrot (Amazona aestiva). Anatomia Histologia Embryologia, 50(1), 192–205. https://doi.org/10.1111/ahe.12618

- Fasola, M., Rubolini, D., Merli, E., Boncompagni, E., & Bressan, U. (2009). Long‐term trends of heron and egret populations in Italy, and the effects of climate, human‐induced mortality, and habitat on population dynamics. Population Ecology, 52(1), 59–72. https://doi.org/10.1007/s10144-009-0165-1

- Franklin, C. E., & Grigg, G. C. (1993). Increased vascularity of the lingual salt glands of the estuarine crocodile, Crocodylus porosus, kept in hyperosmotic salinity. Journal of Morphology, 218(2), 143–151. https://doi.org/10.1002/jmor.1052180204

- Franz-Odendaal, T. A. (2006). Intramembranous ossification of scleral ossicles in Chelydra serpentina. Zoology, 109(1), 75–81. https://doi.org/10.1016/j.zool.2005.10.001

- Fumero-Hernández, M., Encinoso, M., Melian, A., Nuez, H. A., Salman, D., & Jaber, J. R. (2023a). Cross Sectional Anatomy and Magnetic Resonance Imaging of the Juvenile Atlantic Puffin Head (Aves, Alcidae, Fratercula arctica). Animals, 13(22), 3434. https://doi.org/10.3390/ani13223434

- Fumero-Hernández, M., Encinoso, M., Melian, A., Nuez, H. A., Salman, D., & Jaber, J. R. (2023b). Cross Sectional Anatomy and Magnetic Resonance Imaging of the Juvenile Atlantic Puffin Head (Aves, Alcidae, Fratercula arctica). Animals, 13(22), 3434. https://doi.org/10.3390/ani13223434

- Garrido, J. R., Molina, B., & Juan Carlos Del Moral. (2011). Las garzas en España: Población reproductora e invernante en 2010-2011 y método de censo. In Ministerio Para La Transición Ecológica Y El Reto Demográfico. SEO/BirdLife.

https://www.miteco.gob.es/content/dam/miteco/es/biodiversidad/temas/inventarios-nacionales/38-garzas_tcm30-207952.pdf

- Garza real - SEO/BirdLife. (2023, February 27). SEO/BirdLife. https://seo.org/ave/garza-real/

- Gatesy, S. M., & Dial, K. P. (1996). LOCOMOTOR MODULES AND THE EVOLUTION OF AVIAN FLIGHT. Evolution, 50(1), 331–340. https://doi.org/10.1111/j.1558-5646.1996.tb04496.x

- Geist, N. R. (2000). Nasal respiratory turbinate function in birds. Physiological and Biochemical Zoology, 73(5), 581–589. https://doi.org/10.1086/317750

- Getty, R. (2004). Sisson y Grossman. Anatomía de los animales domésticos (5th ed., Vol. 2). Masson. https://veggievet2.wordpress.com/wp-content/uploads/2017/03/anatomia-de-los-animales-domesticosrobert-gettytomo-2.pdf

- Gibbs, C., Lane, J. G., & Denny, H. R. (1979). Radiological features of intra‐nasal lesions in the dog: a review of 100 cases. Journal of Small Animal Practice, 20(9), 515–535. https://doi.org/10.1111/j.1748-5827.1979.tb06760.x

- Grey Heron | BTO. (n.d.). https://www.bto.org/learn/about-birds/birdfacts/grey-heron

- Grosell, M., Heuer, R. M., Wu, N. C., Cramp, R. L., Wang, Y., Mager, E. M., Dwyer, R. G., & Franklin, C. E. (2020). Salt-water acclimation of the estuarine crocodile Crocodylus porosus involves enhanced ion transport properties of the urodaeum and rectum. Journal of Experimental Biology. https://doi.org/10.1242/jeb.210732

- Guo, M., Liu, D., Chen, X., Wu, Y., & Zhang, X. (2021). Pathogenicity and innate response to Avibacterium paragallinarum in chickens. Poultry Science, 101(1), 101523. https://doi.org/10.1016/j.psj.2021.101523

- Hadden, P. W., Ober, W. C., Gerneke, D. A., Thomas, D., Scadeng, M., McGhee, C. N. J., & Zhang, J. (2022). Micro‐CT guided illustration of the head anatomy of penguins (Aves: Sphenisciformes: Spheniscidae). Journal of Morphology, 283(6), 827–851. https://doi.org/10.1002/jmor.21476

- Jones, M. E. H., Button, D. J., Barrett, P. M., & Porro, L. B. (2019). Digital dissection of the head of the rock dove (Columba livia) using contrast-enhanced computed tomography. Zoological Letters, 5(1). https://doi.org/10.1186/s40851-019-0129-z

- Kazemi, S., Rezaei, M., Alizadeh, S., & Hosseinchi, M. (2025). Computed Tomographic Anatomy of the Head in Cockatiel (Nymphicus hollandicus). Veterinary Medicine and Science, 11(2). https://doi.org/10.1002/vms3.70234

- König, H. E., Korbel, R., Liebich, H., & Klupiec, C. (2014). Avian Anatomy: Textbook and Colour Atlas (2nd ed.). 5m.

- Kvarnemo, C., Anderstedt, A., Strandh, M., & Blomqvist, D. (2025). The Importance of Olfaction for Mixed Paternity in Birds. Ecology and Evolution, 15(1). https://doi.org/10.1002/ece3.70863

- Lauridsen, H., Hansen, K., Wang, T., Agger, P., Andersen, J. L., Knudsen, P. S., Rasmussen, A. S., Uhrenholt, L., & Pedersen, M. (2011). Inside out: modern imaging techniques to reveal animal anatomy. PLoS ONE, 6(3), e17879. https://doi.org/10.1371/journal.pone.0017879

- Madkour, F. (2019). Anatomical descriptions of the nasal cavity of the Aquatic and Non-Aquatic birds. SVU- International Journal of Veterinary Sciences, 2(2), 101–110. https://doi.org/10.21608/svu.2019.14982.1022

- Mahmoud, F. A., Gadel-Rab, A. G., & Shawki, N. A. (2018). Functional morphological study of the choana in different bird species. The Journal of Basic and Applied Zoology, 79(1). https://doi.org/10.1186/s41936-018-0026-6

- Martin, G. R. (2011). Through birds' eyes: insights into avian sensory ecology. Journal of Ornithology, 153(S1), 23–48. https://doi.org/10.1007/s10336-011-0771-5

- Martínez, E. D., Espinosa, A. A., Laguía, M. S., Florenciano, M. D. A., Kilroy, D., García, M. I. G., Gomariz, F. M., Collado, C. S., Cano, F. G., Jaber, J. R., & Zarzosa, G. R. (2024). The bony nasal cavity and paranasal sinuses of big felids and domestic cat: a study Using anatomical techniques, computed tomographic images reconstructed in Maximum-Intensity projection, volume rendering and 3D printing models. Animals, 14(17), 2609. https://doi.org/10.3390/ani14172609

- Martínez, E. D., Espinosa, A. A., Laguía, M. S., Kilroy, D., Gomariz, F. M., García, D. L. C., Collado, C. S., Cano, F. G., Jaber, J. R., & Zarzosa, G. R. (2024). An Anatomical Study Using Computed Tomography, Magnetic Resonance Imaging, and Rhinoscopy of the Nasal Cavity of Domestic Cat (Felis silvestris catus L.) and Big Cats: Lion (Panthera leo leo L.), Leopard (Panthera pardus kotiya L.), and Cheetah (Acinonyx jubatus jubatus S.). Animals, 14(8), 1172. https://doi.org/10.3390/ani14081172

- Morales-Espino, A., Déniz, S., Paz-Oliva, P., Roldán-Medina, N., Encinoso, M., Suárez-Cabrera, F., & Jaber, J. R. (2024). Cory's Shearwater (Calonectris borealis): Exploring Normal Head Anatomy through Cross-Sectional Anatomy, Computed Tomography and Magnetic Resonance Imaging. Animals, 14(13), 1962. https://doi.org/10.3390/ani14131962

- Morales-Espino, A., Fumero-Hernández, M., Suárez-Cabrera, F., Encinoso, M., Conde-Felipe, M. M., & Jaber, J. R. (2024). Computed Tomography Anatomy of the Juvenile Cory's Shearwater (Calonectris borealis) Normal Nasal Cavity. Animals, 14(20), 3015. https://doi.org/10.3390/ani14203015

- Morr, A. J. (2023, September 26). Did you know: Birds Beaks Adapt to food. SIB. https://seabrookislandbirders.org/2023/09/28/did-you-know-birds-beaks-adapt-to-food/

- Ogórek, R., Borzęcka, J., Kłosińska, K., Piecuch, A., Przymencki, M., Litwiniak, K., & Suchodolski, J. (2022). A Culture-Based Study of Micromycetes Isolated from the Urban Nests of Grey Heron (*Ardea cinerea*) in SW Poland. Animals, 12(6), 676. https://doi.org/10.3390/ani12060676

- Orosz, S. E., & Lichtenberger, M. (2011). Avian Respiratory distress: Etiology, diagnosis, and treatment. Veterinary Clinics of North America Exotic Animal Practice, 14(2), 241–255. https://doi.org/10.1016/j.cvex.2011.03.003

- Papes, F., Logan, D. W., & Stowers, L. (2010). The Vomeronasal Organ Mediates Interspecies Defensive Behaviors through Detection of Protein Pheromone Homologs. Cell, 141(4), 692–703. https://doi.org/10.1016/j.cell.2010.03.037

- Porter, W. R., & Witmer, L. M. (2016). Avian cephalic vascular anatomy, sites of thermal exchange, and the Rete Ophthalmicum. The Anatomical Record, 299(11), 1461–1486. https://doi.org/10.1002/ar.23375

- Quesada-Canales, Ó., Díaz-Delgado, J., Paz, Y., Domínguez, L., Bezos, J., Calabuig, P., Suárez-Bonnet, A., Fernández, A., & Andrada, M. (2013). Disseminated Avian Mycobacteriosis in a Free-Living Grey Heron (*Ardea cinerea*). Avian Diseases, 57(3), 703–706. https://doi.org/10.1637/10474-122612-case.1

- Redacción. (2023, January 18). Confirman varios casos de gripe aviar en aves de parques de Barcelona. Animal´S Health. https://www.animalshealth.es/avicultura/confirman-varios-casos-gripe-aviar-aves-parques-barcelona

- Sandoval, J. (2000). Tratado de anatomía veterinaria: Cabeza y Sistemas viscerales: Vol. Tomo III. Imprenta Sorles.

- Schwarz, T., Sullivan, M., & Hartung, K. (2000). RADIOGRAPHIC DETECTION OF DEFECTS OF THE NASAL BOUNDARIES. Veterinary Radiology & Ultrasound, 41(3), 226–230. https://doi.org/10.1111/j.1740-8261.2000.tb01483.x

- Shuttleworth, T. J., Thompson, J. L., & Dantzler, W. H. (1987). Potassium secretion by nasal salt glands of desert lizard Sauromalus obesus. AJP Regulatory Integrative and Comparative Physiology, 253(1), R83–R90. https://doi.org/10.1152/ajpregu.1987.253.1.r83

- Sovrano, L. V., Beltzer, A. H., Regner, S. A., Giraudo, A. R., Colombo, V. C., Perusini, R., Saravia-Pietropaolo, M. J., Arce, S. I., Ruiz, M. F., & Beldomenico, P. M. (2019). Inusual mortandad de pichones y juveniles de Garza Bruja Nycticorax nycticorax (Ardeidae) en una nueva colonia nidificante en el centro de Argentina. Caldasia, 41(2), 257–267. https://doi.org/10.15446/caldasia.v41n2.71255

- Stańczyk, E. K., Gallego, M. L. V., Nowak, M., Hatt, J., Kircher, P. R., & Carrera, I. (2018a). 3.0 Tesla magnetic resonance imaging anatomy of the central nervous system, eye, and inner ear in birds of prey. Veterinary Radiology & Ultrasound, 59(6), 705–714. https://doi.org/10.1111/vru.12657

- Starck, J. M. (1995). Comparative anatomy of the external and middle ear of palaeognathous birds. Advances in Anatomy, Embryology and Cell Biology. https://doi.org/10.1007/978-3-642-79592-3

- Swayne, D. E. (2023, June 6). Influenza aviar. Manual De Veterinaria De MSD. https://www.msdvetmanual.com/es/avicultura/influenza-aviar/influenza-aviar

- Veladiano, I. A., Banzato, T., Bellini, L., Montani, A., Catania, S., & Zotti, A. (2016). Computed tomographic anatomy of the heads of blue-and-gold macaws

  (Ara ararauna), African grey parrots (Psittacus erithacus), and monk parakeets (Myiopsitta monachus). American Journal of Veterinary Research, 77(12), 1346–1356. https://doi.org/10.2460/ajvr.77.12.1346

- Wild, J. M., & Zeigler, H. P. (1996). Central projections and somatotopic organisation of trigeminal primary afferents in pigeon (Columba livia). The Journal of Comparative Neurology. https://doi.org/10.1002/(SICI)1096-9861(19960422)368:1%3C136::AID-CNE9%3E3.0.CO;2-4

- Williams, M. N., & Wild, J. (2001). Trigeminal innervated iron-containing structures in the beak of homing pigeons, and other birds. Brain Research, 889(1–2), 243–246. https://doi.org/10.1016/s0006-8993(00)03114-0

- Wilson, M., Mauragis, D., & Berry, C. R. (2014). Small animal skull & nasofacial radiography,including the nasal cavity & frontal sinuses: University of Florida. Today's Veterinary Practice. https://imaging.vetmed.ufl.edu/files/2016/06/Small-Animal-Skull-Nasofacial-Radiography-Including-the-Nasal-Cavity-Frontal-Sinuses.pdf

- Yokosuka, M., Hagiwara, A., Saito, T. R., Tsukahara, N., Aoyama, M., Wakabayashi, Y., Sugita, S., & Ichikawa, M. (2009). Histological Properties of the Nasal Cavity and Olfactory Bulb of the Japanese Jungle Crow Corvus macrorhynchos. Chemical Senses, 34(7), 581–593. https://doi.org/10.1093/chemse/bjp040